

Part-per-million quantization and current-induced breakdown of the quantum anomalous Hall effect

E. J. Fox,^{1,2} I. T. Rosen,^{2,3} Yanfei Yang,⁴ George R. Jones,⁴ Randolph E. Elmquist,⁴ Xufeng Kou,^{5,6} Lei Pan,⁵ Kang L. Wang,⁵ and D. Goldhaber-Gordon^{1,2,*}

¹*Department of Physics, Stanford University, Stanford, California 94305, USA*

²*Stanford Institute for Materials and Energy Sciences, SLAC National Accelerator Laboratory, 2575 Sand Hill Road, Menlo Park, California 94025, USA*

³*Department of Applied Physics, Stanford University, Stanford, California 94305, USA*

⁴*National Institute of Standards and Technology (NIST), Gaithersburg, Maryland 20899-8171, USA*

⁵*Department of Electrical Engineering, University of California, Los Angeles, California 90095, USA*

⁶*School of Information Science and Technology, ShanghaiTech University 201210, China*



(Received 20 September 2017; revised manuscript received 12 May 2018; published 27 August 2018)

In the quantum anomalous Hall effect, quantized Hall resistance and vanishing longitudinal resistivity are predicted to result from the presence of dissipationless, chiral edge states and an insulating two-dimensional bulk, without requiring an external magnetic field. Here, we explore the potential of this effect in magnetic topological insulator thin films for metrological applications. Using a cryogenic current comparator system, we measure quantization of the Hall resistance to within one part per million and, at lower current bias, longitudinal resistivity under 10 m Ω at zero magnetic field. Increasing the current density past a critical value leads to a breakdown of the quantized, low-dissipation state, which we attribute to electron heating in bulk current flow. We further investigate the prebreakdown regime by measuring transport dependence on temperature, current, and geometry, and find evidence for bulk dissipation, including thermal activation and possible variable-range hopping.

DOI: [10.1103/PhysRevB.98.075145](https://doi.org/10.1103/PhysRevB.98.075145)

I. INTRODUCTION

When doped with certain transition metals, chalcogenide-based three-dimensional (3D) topological insulators (TIs) can be made ferromagnetic, breaking time-reversal symmetry and opening a gap in the Dirac spectrum of the topological surface states [1–3]. However, this gap should close where the component of the magnetization normal to the surface changes direction. In a thin-film sample uniformly magnetized in the out-of-plane direction, this transition occurs at the physical edge of the film as the surface normal switches direction in going from the top surface to the bottom. In the idealized theoretical picture of these systems, the 2D bulk is completely gapped, and one-dimensional channels arising at such boundaries are chiral and dissipationless due to the absence of available states for backscattering. The resulting edge conduction, which does not require an external magnetic field, is known as the quantum anomalous Hall (QAH) effect, and transport measurements are predicted to find vanishing longitudinal resistivity $\rho_{xx} = 0$ accompanied by quantized Hall resistivity $\rho_{yx} = \pm h/e^2$, where h is Planck's constant and e the electron charge.

Experiments have indeed found $\rho_{yx} \approx h/e^2$ but have not clearly demonstrated an insulating bulk as predicted. The first reported observation of QAH in Cr-doped (Bi,Sb)₂Te₃ at zero field measured ρ_{yx} within a few percent of h/e^2 , yet $\rho_{xx} \approx 2.5$ k Ω [4], far above the expected value. Subsequent works on

the same material system [5–9] and a V-doped analog [10,11] have replicated the effect, progressively improving on the degree of quantization and reducing longitudinal resistivity, but in all cases have found nonvanishing ρ_{xx} , indicating dissipative transport. Proposed explanations for this dissipation include thermally activated bulk or surface carriers [7], variable-range hopping (VRH) [4,12], or the presence of extra, nonchiral edge states [6,13,14]. Moreover, ρ_{yx} deviates from quantization and ρ_{xx} rises rapidly with temperature, typically on a scale of hundreds of millikelvin [7,12,14,15], unexpectedly small compared to the Curie temperature, which is generally tens of kelvin [3–6,8–11,16,17]. Angle-resolved photoemission spectroscopy results [17] suggest that in V-doped films, this discrepancy may be due to the bulk valence band overlapping the surface-state gap, while scanning tunneling microscopy [16] on Cr-doped bulk crystals shows strong spatial variations of the exchange-induced gap which could result in a small temperature scale in transport [18], despite an average gap size of ~ 30 meV. However, a comprehensive explanation of the unexpected and nonideal behavior in QAH is still lacking.

To investigate the degree to which dissipation can be removed, several studies [7,10,15] previously attempted to characterize samples with apparently well-quantized Hall resistance at temperatures of tens of millikelvin. The most precise of these measurements show $\rho_{yx} = h/e^2$ to within one part in 10^4 and ρ_{xx} as low as 1 Ω [7]. In contrast, measurements of the quantum Hall (QH) effect, in which similar vanishing ρ_{xx} and quantized $\rho_{yx} = h/\nu e^2$ for integer ν is predicted due to Landau level formation, have found quantization of the Hall resistance to within a part in 10^9 and the lowest longitudinal

*To whom correspondence should be addressed: goldhaber-gordon@stanford.edu

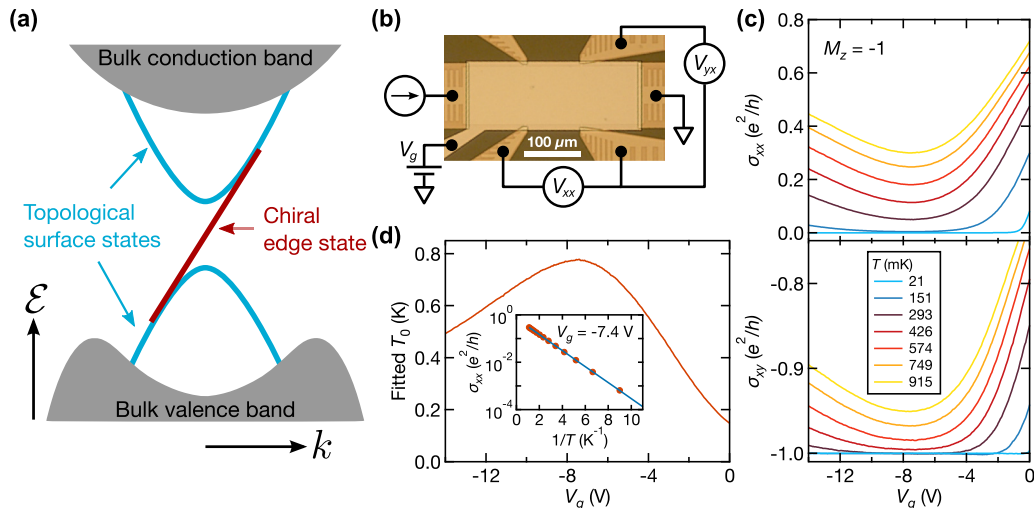


FIG. 1. QAH device and dependence of conductivity on gate voltage and temperature. (a) Schematic band structure diagram of a magnetic topological insulator in the QAH state, where \mathcal{E} is energy and k the wave vector. A gapless chiral edge state is hosted in the exchange-induced gap in the Dirac spectrum of the topological surface states inside the 3D bulk gap. Quantization of the Hall resistance is expected when the Fermi level is in the surface-state gap. (b) Micrograph of top-gated Hall bar based on 6-nm-thick film of $(\text{Cr}_{0.12}\text{Bi}_{0.26}\text{Sb}_{0.62})_2\text{Te}_3$. A simplified schematic of the measurement scheme is overlaid. (c) Longitudinal and transverse conductivities of device 1, σ_{xx} and σ_{xy} , respectively, derived from lock-in amplifier measurements of the resistivity as a function of gate voltage V_g for temperatures between 21 and 915 mK. At the lowest temperatures, the conductivities plateau over a wide range in V_g at values consistent with $\sigma_{xy} = -e^2/h$ and $\sigma_{xx} \approx 0$ to within expected experimental error. (d) Fitted temperature scale T_0 for thermally activated conduction, $\sigma_{xx} \propto e^{-T_0/T}$, as a function of V_g in device 1, peaking at 780 mK. Inset, an Arrhenius plot of σ_{xx} as a function of $1/T$ at $V_g = -7.4$ V with a fit (blue line) to thermal activation.

resistivity ever measured in a nonsuperconducting sample [19]. Because of the precision and reproducibility of such measurements, a conventional value of the von Klitzing constant $R_K = h/e^2$ is the basis for practical metrology of the ohm, even though maintaining a QH resistance standard [20] requires very low cryogenic temperatures and large magnetic fields. The situation is however improving; in graphene, resistance quantization to within one part in 10^9 can be measured at 5 K in a 5-T field [21].

Realization of the QAH effect raises the prospect of a future quantum resistance standard without need for a large superconducting solenoid. Beyond making such standards more economical and portable, this could allow combining a resistance standard in a single cryostat with a cryogenic current comparator and other components of the quantum metrology triangle [22,23]. Such a combination recently achieved world-record precision for a current source [24] but required three separate cryostats. While dilution refrigerator temperatures are currently needed to observe quantization of the Hall resistance in QAH systems, elucidation of dissipation mechanisms and materials development may point the way toward increasing practicality. Examinations of film thickness dependence [25], alternative magnetic dopants [10,11], and growth techniques have begun to explore a range of possibilities, with a modulation-doped film in particular exhibiting $\rho_{yx} = 0.97 h/e^2$ even at 2 K [9]. Also, theoretical proposals already exist for materials that could exhibit QAH near room temperature [26,27]. With this in mind, it is worth exploring the quantization and dissipation in existing materials to understand potential limitations.

Here, we present the most precise measurements reported to date of the Hall resistance in a QAH system, finding quantization to within a part in 10^6 of h/e^2 and, at lower current bias,

longitudinal resistivity under 10 m Ω . Deviating from optimal conditions allows us to explore the nature of the dissipation in this system to understand ways to improve this performance further. In particular, we find that increasing the current density beyond a critical value causes a rapid rise in dissipation, echoing the breakdown phenomenon in the QH effect.

II. QUANTIZATION OF THE HALL RESISTANCE

We performed our study of the QAH effect with a six-quintuple-layer sample of $(\text{Cr}_{0.12}\text{Bi}_{0.26}\text{Sb}_{0.62})_2\text{Te}_3$ grown on a GaAs substrate by molecular beam epitaxy. Using photolithography, we fabricated a Hall bar (device 1), 100 μm wide with a 100 μm center-to-center distance between 2- μm -wide voltage terminals [Fig. 1(b)]. The film was etched with Ar ion milling to define a mesa, and 5 nm/100 nm, Ti/Au ohmic contacts were deposited by e-beam evaporation. After growing a 40-nm Al_2O_3 dielectric over the entire sample by atomic layer deposition, we patterned and deposited a Ti/Au gate, which allows tuning of the chemical potential in the film. Finally, we removed the remaining uncovered alumina with a chemical etch before wire bonding.

A. Initial characterization

To observe QAH, we first measured $\rho_{xx} = V_{xx}/I$ and $\rho_{yx} = V_{yx}/I$ using standard lock-in amplifier techniques with a 5-nA bias current and the sample cooled to 21 mK in a dilution refrigerator. After magnetizing the film by applying a field $\mu_0 H = -0.5$ T and then reducing the applied field to zero, $\rho_{xx} \approx 1$ k Ω and $|\rho_{yx}| \approx 0.997 e^2/h$ with the gate grounded. Tuning the gate voltage V_g , we found a wide plateau where ρ_{yx} is constant to within two parts in 10^4 and ρ_{xx} vanishes to

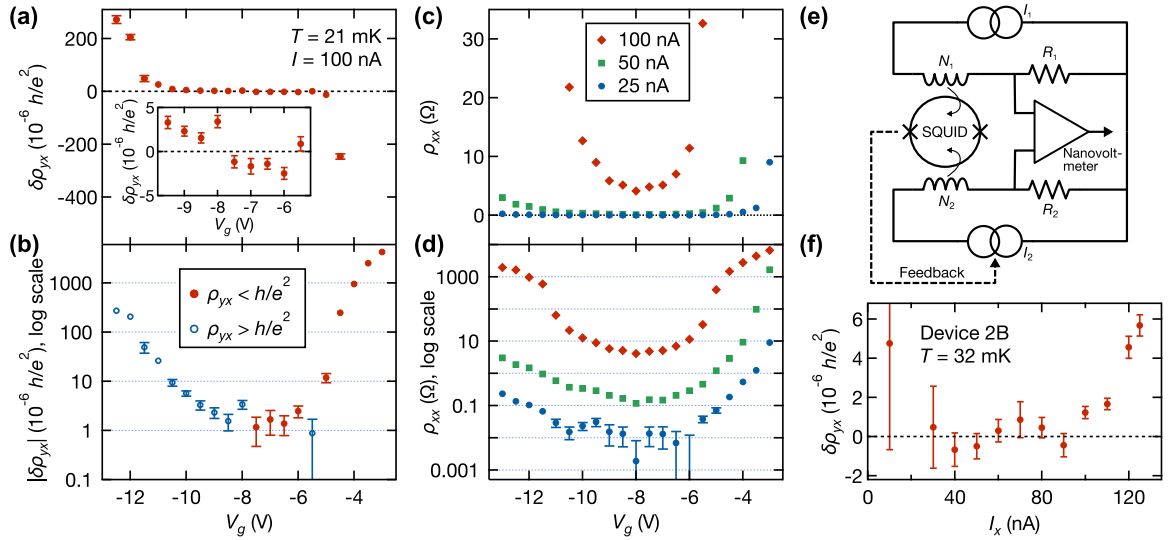


FIG. 2. Cryogenic current comparator measurements. (a) Precise measurements of ρ_{yx} in device 1 using a 100-nA current at 21 mK show a plateau of $\delta\rho_{yx} = |\rho_{yx}| - h/e^2 \approx 0$ for a range of V_g , indicating the accuracy of quantization. Inset, a zoomed-in view of the Hall resistance deviations in the center of the plateau. In (b), the same data are plotted as $|\delta\rho_{yx}|$ on a log scale. (c, d) ρ_{xx} of device 1 measured as a function of V_g for three different bias currents shows strong current and gate voltage dependence, displayed on linear (c) and log (d) scales. At 25 nA with V_g near the center of the plateau, the resistivity is near vanishing and measurements approach the noise floor. (e) Simplified schematic of the cryogenic current comparator. (f) Measurements of $\delta\rho_{yx}$ in a different Hall bar (device 2B) as a function of current I_x , showing accurate quantization for $I_x \leq 90$ nA. In all plots, error bars show the standard uncertainty and are omitted when smaller than the marker.

the accuracy of our measurement, from which we infer ρ_{yx} is accurately quantized at $-h/e^2$ (this is verified later). More specifically, lock-in measurements yielded $\rho_{xx} \approx 9 \Omega$ between the voltage terminals adjacent to the source in the clockwise direction around the edge, the direction of edge state chirality in this configuration [7], and $\rho_{xx} \approx -1 \Omega$ on the opposite side. These nonzero values are consistent with systematic error due to leakage currents into the voltage preamplifiers [7,28], which have 100-M Ω input impedances. With the sample magnetized, the contact resistances were determined to be under $\sim 2 \Omega$ for the source and drain and below $\sim 10 \Omega$ for the voltage terminals, which should be sufficiently small to avoid any non-negligible systematic perturbations in the measured resistances at the level of precision in this work [29].

By heating the sample above base temperature, we observed the onset of dissipation, shown in Fig. 1(c) in terms of the longitudinal conductivity $\sigma_{xx} = \rho_{xx}/(\rho_{xx}^2 + \rho_{yx}^2)$ and transverse conductivity $\sigma_{xy} = \rho_{yx}/(\rho_{xx}^2 + \rho_{yx}^2)$. Within the plateau, the conductivity appears thermally activated, with $\sigma_{xx} \propto e^{-T_0/T}$ when larger than the systematic offsets due to leakage currents. The fitted thermal activation temperature scale T_0 , shown in Fig. 1(d), peaks at 780 mK with $V_g = -7.4$ V, indicating that we can tune the Fermi level through the apparent center of the gap. [A schematic band structure diagram is shown in Fig. 1(a).] If the thermal activation fit held to our lowest temperatures, we would expect to find $\sigma_{xx} < 10^{-15} e^2/h$ and correspondingly small deviations from quantization, assuming behavior similar to QH [40], but measuring this is far beyond the capabilities of our standard lock-in methods.

B. Precision measurements

To overcome the limitations in precision of the lock-in setup, we turned to measuring with a cryogenic current comparator

(CCC), a device typically used in quantum Hall metrology [20]. A simplified schematic of a CCC is shown in Fig. 2(e). With this instrument, two low-noise current sources drive currents I_1 and I_2 through two resistors R_1 and R_2 which are to be compared. The ratio of currents is precisely balanced by using windings that are inductively coupled to a superconducting quantum interference device (SQUID). The measurement of the net flux with the SQUID produces a feedback signal that keeps the net flux constant and thereby holds the ratio of the two currents fixed according to the relation $I_1 N_1 = I_2 N_2$, where N_1 and N_2 are the numbers of windings in each current loop. With the proper choice of N_1 and N_2 , the voltage drops across R_1 and R_2 are approximately the same, and the difference $V = I_1 R_1 - I_2 R_2$ is measured with a nanovoltmeter. In this way, a precise measurement of the ratio of the two resistors is obtained.

Using a commercial CCC system [41,42], we compared the Hall resistance of our magnetic TI Hall bar with a 100- Ω resistance standard calibrated at the National Institute of Standards and Technology (NIST), shipped to Stanford, and later remeasured at NIST to confirm accuracy to within one part in 10^7 . Measuring with a 100-nA current across the Hall bar, we observed a plateau in the deviation of the Hall resistance from quantization $\delta\rho_{yx} = |\rho_{yx}| - h/e^2$ as a function of V_g , shown on a linear scale in Fig. 2(a) and log scale in Fig. 2(b). [Each plotted data point represents ~ 60 individual measurements [29] and error bars show the standard uncertainty.] Within the plateau, for V_g between -5.5 V and -9.5 V, ρ_{yx} is quantized to within $4 \times 10^{-6} h/e^2$ [Fig. 2(a), inset], whereas approaching the plateau edges $|\delta\rho_{yx}|$ grows approximately exponentially with V_g . Near the center of the plateau, there appears to be a small but nonzero negative slope in $\delta\rho_{yx}$ with V_g ; this is likely related to the dissipation (discussed below) still present at a current of 100 nA.

We would expect $\delta\rho_{yx} < 0$ in the presence of dissipation, as homogeneous bulk conduction should reduce the Hall voltage by allowing transverse current to flow across the Hall bar. Likewise, conduction via additional nonchiral edge states would reduce the measured Hall resistance [13]. Counter to this expectation, as V_g was tuned to the left side of the ρ_{yx} plateau we observed positive $\delta\rho_{yx}$ as the deviation from quantization increased [Fig. 2(b)]. Similar anomalous “overshoot” of the quantized value for the Hall resistance can sometimes be seen in the QH effect when the current splits between multiple (evanescent) incompressible strips of different filling factors that are narrower than the Fermi wavelength [43], or when geometric effects lead to mixing of ρ_{xx} into ρ_{yx} [44]. The former case has no clear analog in QAH, where a single edge state is predicted. We speculate that this behavior results from spatially inhomogeneous bulk conduction [29] and would be reversed with increased dissipation [at higher temperatures, e.g., as in Fig. 1(c)], though further investigation is required to clarify this point.

For an additional check of the CCC and resistance standard calibration, we measured an epitaxial graphene [45] sample designed to provide an h/e^2 resistance. The device consists of a pair of triple-series-connected Hall bars [46,47]. When the graphene is tuned to a $\nu = 2$ quantum Hall state, a quasi-Hall voltage can be measured between voltage leads on the two Hall bars that gives a four-terminal resistance of h/e^2 . With 1 μA across the graphene device and an applied field $\mu_0 H = -6\text{ T}$, we observed this four-terminal resistance with equivalent $\delta\rho_{yx} = (-6.5 \pm 4.6) \times 10^{-8} h/e^2$, confirming the calibration of the resistance standard to well beyond the accuracy with which we measured quantization in the QAH device. To verify proper operation of the CCC at the lower currents used for QAH, we also measured the graphene device at 100 nA and found quantization with $\delta\rho_{yx} = (1.9 \pm 4.0) \times 10^{-7} h/e^2$ using 120 individual measurements.

Using the CCC’s nanovoltmeter, which has $\sim 100\text{ G}\Omega$ input impedance [48], we separately measured ρ_{xx} in the magnetic TI Hall bar for the same range of V_g . Viewed on a linear scale in Fig. 2(c), there is a clear plateau near $\rho_{xx} = 0$ at gate voltages for which ρ_{yx} is well quantized and a sharp rise as V_g is tuned outside the central region. However, at 100 nA, the same current at which ρ_{yx} was measured for Figs. 2(a) and 2(b), we surprisingly found ρ_{xx} still above $4\ \Omega$ at minimum. The same measurements with lower current, 50 nA and 25 nA, plotted in Figs. 2(c) and 2(d), show the strong current dependence of the dissipation in this range, with ρ_{xx} at 25 nA between 2 and 4 orders of magnitude lower than at 100 nA, and a minimum value of $\rho_{xx} = 1.9 \pm 6.2\ \text{m}\Omega$ at $V_g = -8\ \text{V}$.

Reducing the bias current increases the noise in Hall measurements but can also lead to improved quantization. On a separate Hall bar (device 2B, see below), we developed a better procedure to extract precisely quantized Hall resistance [29]. At an elevated temperature (370 mK), we measured ρ_{xx} as a function of V_g with the sample magnetized. For subsequent measurements, we set the gate voltage at the value minimizing ρ_{xx} ($-5.8\ \text{V}$). The minimum in ρ_{xx} should roughly correspond to a maximum in the thermal activation scale T_0 , where we expect to find minimal dissipation. (In device 1, the peak in T_0 is within 0.05 V of the gate voltage minimizing ρ_{xx} at a similar temperature of 358 mK.) No attempt was made to fine-tune

this gate voltage in response to Hall resistance measurements. Then at base temperature (32 mK in this case), we measured the current dependence of $\delta\rho_{yx}$, shown in Fig. 2(f), to optimize the tradeoff between noise and accuracy. (Longitudinal resistivity measurements from this device can be seen in Fig. 3(d) and in the Supplemental Material [29].) At 100 nA and above, there appear to be consistent deviations in ρ_{yx} from h/e^2 . However, there is no clear trend at lower currents, so combining these measurements can give a reasonable estimate of ρ_{yx} . Averaging the Hall measurements for currents $I_x \leq 90\ \text{nA}$, where $\rho_{xx} < 1.5\ \Omega$ [29], weighted by the inverse variance of the mean, yields $\delta\rho_{yx} = (0.04 \pm 0.26) \times 10^{-6} h/e^2$.

III. CURRENT-INDUCED BREAKDOWN

To further investigate the strong current dependence, we measured V_{xx} for currents I_x between 25 nA and 350 nA with the gate tuned near the center of the plateau, $V_g = -7.5\ \text{V}$. The relationship between V_{xx} and I_x , shown on a log-scale plot in Fig. 3(a) or as $\rho_{xx} = V_{xx}/I_x$ versus I_x in Fig. 3(b), is markedly nonlinear. At base temperature in particular, we find an abrupt increase in longitudinal resistivity reminiscent of the current-induced breakdown of the QH effect [49]. Although this rise in ρ_{xx} is not as sharp as is usually observed in QH breakdown, here ρ_{xx} nonetheless increases by more than a factor of 22 as the current is increased by 20% starting at $I_x = 125\ \text{nA}$.

At higher temperatures, the breakdown effect is smeared out. Data taken at 203 mK, displayed in Figs. 3(a) and 3(b), indicate ρ_{xx} is relatively temperature independent at higher currents in the breakdown regime, while at lower currents the traces taken at different temperatures diverge significantly. A smoother current dependence of similar form to that seen at 203 mK was recently observed in a QAH system by Kawamura *et al.* [12], who attributed the behavior to electric-field-driven VRH at low temperatures. Here, the development of a sharp rise in $\rho_{xx}(I_x)$ at low temperatures instead suggests the bootstrap electron heating (BSEH) model of QH breakdown [50] may explain breakdown behavior in QAH as well.

A. Breakdown via bootstrap electron heating

The BSEH model ascribes the sharp increase in dissipation to runaway heating of the electron system, whose temperature T_e diverges from the lattice temperature T_L to settle in a steady state in which energy gain and loss rates are balanced, as given by the equation [50]

$$\sigma_{xx} E_y^2 = \frac{Z(T_e) - Z(T_L)}{\tau}, \quad (1)$$

where $Z(T)$ is the areal energy density of the electron system at temperature T and τ is the temperature-dependent electron energy relaxation time. The transverse electric field E_y is related to the current density j_x by $E_y = \rho_{yx} j_x$, and at currents relevant for breakdown, the average field $E_y \approx j_x h/e^2$. The left-hand side of Eq. (1) is the rate of energy gain per unit area $G = j \cdot E = \sigma_{xx} E^2 \approx \sigma_{xx} E_y^2$ since $E_y \gg E_x$, while the right-hand side gives the rate L of energy loss to the lattice per area. The strong T_e dependence of the conductivity enables “bootstrap” heating of the electron system when the current is increased enough to cause this balance to become unstable, with $\partial G/\partial T_e > \partial L/\partial T_e$, until a new stable equilibrium is

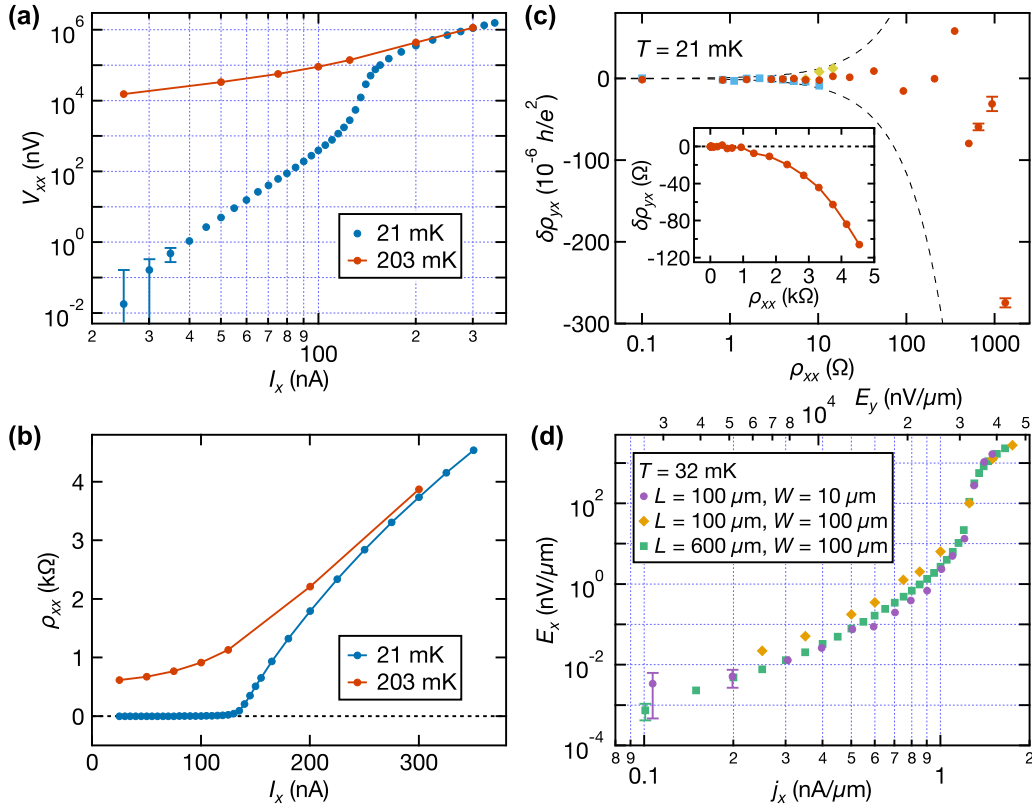


FIG. 3. Current-induced breakdown of the QAH effect. (a) Longitudinal voltage V_{xx} in device 1 measured with the nanovoltmeter as a function of bias current I_x with $V_g = -7.5$ V, shown for lattice temperatures of 21 mK and 203 mK as measured by the mixing chamber plate thermometer. At base temperature and $I_x \leq 100$ nA, we observe an apparent power law $V_{xx} \propto I_x^{6.4}$. After a sharp rise in V_{xx} for $T = 21$ mK starting at around $I_x = 125$ nA, the curves for the two temperatures nearly overlap, consistent with runaway electron heating. (b) ρ_{xx} of device 1 calculated from the data in (a), shown on a linear plot versus I_x . (c) Hall resistance deviations $\delta\rho_{yx}$ of device 1, measured on three separate upward sweeps of current (shown with different colors and symbols—data shown in blue and yellow were taken on the opposite pair of voltage contacts from that in red), plotted against separate measurements of ρ_{xx} from (b). Almost all points below $\rho_{xx} = 1$ k Ω , where $|\delta\rho_{yx}| < 10^{-4} e^2/h$, fall within $|\delta\rho_{yx}| < 0.03\rho_{xx}$, shown by the dashed lines. A detailed view of the data with low ρ_{xx} is given in the Supplemental Material [29]. (Inset) $\delta\rho_{yx}$ exhibits quadratic dependence on ρ_{xx} at higher dissipation. (d) Longitudinal electric field E_x vs current density j_x for three Hall bars of varying size (devices 2A–2C), each at their optimum gate voltage, showing geometry-independent behavior at high current density and similar behavior even at low current density. The average transverse electric field $E_y = \rho_{yx}j_x$ shown on the top axis is calculated assuming $\rho_{yx} = h/e^2$.

found at higher T_e . In a QH system, this is thought to occur through an avalanche multiplication of excited carriers by inter-Landau-level impact ionization [50]; a similar process could take place in the QAH effect with the surface-state bands in place of Landau levels. At sufficiently low temperature, this effect can be observed in QH as a discontinuous jump in σ_{xx} with increasing j_x .

In our QAH measurements, we instead find a sharp but continuous rise, but this is consistent with QH experiments at higher temperatures [51] and the BSEH model, which predicts a continuous transition when $k_B T_L$ exceeds $\sim 6\%$ of the gap between Landau levels. Though the sample appears to reach $k_B T_L/2\Delta \approx 0.014$ at a 21 mK base temperature, where $2\Delta = 2k_B T_0 \approx 130 \mu\text{eV}$ is the gap extracted from thermal activation, the lack of a discontinuous jump could reflect differences in the form of $Z(T)$, with a gapped Dirac band structure in place of sharp Landau levels, and in energy relaxation processes. Additional electron heating due to electronic noise, known to generically cause T_e to diverge from T_L at the lowest temperatures reachable with dilution refrigerators, could also contribute to smoothing, whereas with larger gaps in QH

systems it may be negligible. At higher temperatures above $\sim 10\%$ of the gap size, the breakdown transition is expected to be entirely smeared out according to the BSEH model, which is indeed what we observe at 203 mK where $k_B T_L/2\Delta \approx 0.13$ [Figs. 3(a) and 3(b)].

B. Possible Zener tunneling

Another mechanism which could plausibly contribute to the breakdown effect is Zener tunneling between the occupied and unoccupied surface-state bands due to the tilted potential from the Hall electric field. An analogous process in QH breakdown, quasielastic inter-Landau-level scattering (QUILLS) [52], is predicted to occur when the Hall electric field is sufficiently strong to cause substantial overlap of the wave functions of states with equal energies in the highest occupied and lowest unoccupied Landau levels. However, in most cases (for wide Hall bars), the QUILLS model significantly overestimates the breakdown current [49,50]. In the QAH system, the onset of strong tunneling should occur roughly when the potential changes by the gap size over the characteristic length scale

$\lambda = \hbar v_F / \Delta$ of the gapped Dirac spectrum, where v_F is the surface-state Fermi velocity. Calculations for Zener tunneling in a one-dimensional gapped Dirac system give a characteristic electric field of $E_0 = \pi \Delta^2 / e \hbar v_F = \pi \Delta / e \lambda$ for this onset [53] (which should be the same in two dimensions [54]). With $v_F \approx 4 \times 10^5$ m/s [55] and the gap extracted from thermal activation, we estimate $\lambda \approx 4 \mu\text{m}$ and $E_0 \approx 50$ V/m, corresponding to a current density of $j_0 \approx 2$ nA/ μm , remarkably close to the measured value of ~ 1.2 nA/ μm for breakdown, assuming uniform current flow in the bulk (discussed below).

However, complications to this picture lead us to believe Zener tunneling may be less significant than the calculation suggests. If the exchange-induced gap fluctuates spatially, the energy scale corresponding to thermal activation in transport measurements may be substantially smaller than the average gap size [18]. If Δ varies strongly over a length scale smaller than $\lambda \approx 4 \mu\text{m}$, estimated from the transport gap, the true value of the onset field E_0 may be far higher due to a larger effective tunnel barrier (noting $E_0 \propto \Delta^2$ in a spatially uniform system). Further, we have not accounted for spin texture of the surface states; the spin state at the valence band maximum should be opposite to that at the conduction band minimum [56,57], which might suppress tunneling.

For these reasons, although we are unable to rule it out, strong Zener tunneling appears less likely to be the mechanism for the sharp breakdown phenomenon than runaway electron heating. We cannot make a quantitative prediction of the breakdown current with BSEH for comparison, mainly due to a lack of information about the energy relaxation time, but the breakdown behavior is otherwise quite consistent with the model, as described earlier. Moreover, the prediction of runaway electron heating by considering heat balance according to Eq. (1) is fairly generic, independent of the microscopic details of the system. Sharp switching between low- and high-resistance states in certain disordered insulators has been attributed to a similar effect [58], for example. Since the conductivity in the QAH system has a strong temperature dependence similar to that in QH, a BSEH-driven breakdown should also occur in the QAH state at sufficiently low temperatures in the absence of another breakdown mechanism. Given our conjecture that strong Zener-tunneling-driven breakdown should require significantly higher current than the observed value, BSEH seems to be the most plausible explanation.

In any case, even if breakdown is caused by BSEH, Zener tunneling is not necessarily entirely absent. In addition to thermal excitations, weak tunneling at lower fields is proposed to contribute to BSEH as one form of fluctuation that can trigger a carrier avalanche heating process in a QH system [50], and could possibly play a similar role here.

C. Relationship between the Hall and longitudinal resistivities

We additionally measured $\delta\rho_{yx}$ for varying currents I_x at 21 mK. Figure 3(c) displays these data parametrically as $\delta\rho_{yx}(I_x)$ versus $\rho_{xx}(I_x)$ from Fig. 3(b). In contrast to the QH effect, where $\delta\rho_{yx} \propto \rho_{xx}$ is typically seen up to $\rho_{xx} \approx 10 \Omega$ [19,40], we do not observe a linear relationship. At intermediate currents in particular, both in the sharp breakdown observed in ρ_{xx} and in the prebreakdown regime (where ρ_{xx} is $\sim 10 \Omega$ or lower), significant fluctuations in $\delta\rho_{yx}$ occur as

the current is varied. These fluctuations are not repeatable: measurements of $\delta\rho_{yx}$ taken at the same value of I_x but on separate sweeps of increasing current often differ by significantly more than the statistical uncertainty of each individual measurement. Nonetheless, the deviations remain surprisingly small compared to ρ_{xx} even during the sharp breakdown, with $|\delta\rho_{yx}| < 8 \times 10^{-5} h/e^2 \approx 2 \Omega$ for $\rho_{xx} < 1$ k Ω . Within this range, almost all measurements satisfy $\delta\rho_{yx} < 0.03\rho_{xx}$, except for some at the lowest values of ρ_{xx} , corresponding to low current, where noise in the Hall measurements affects the ratio more significantly. [A detailed view of Fig. 3(c) is included in the Supplemental Material [29].] It is unclear whether this relationship holds as the current tends to zero, but it would suggest that $\delta\rho_{yx} < 10^{-6} h/e^2$ for ρ_{xx} below $\sim 1 \Omega$. For thermally driven deviations, on the other hand, lock-in measurements at 5 nA give a significantly larger $\delta\rho_{yx}$ of -33Ω when $\rho_{xx} = 704 \Omega$ at $T = 240$ mK.

A possible explanation for this behavior could be spatially inhomogeneous dissipation near current-induced breakdown, leading to enhanced ρ_{xx} with lesser impact on ρ_{yx} [59], with fluctuations as the net current is increased caused by changes in the spatial distribution of dissipative current flow. As increasing current drives ρ_{xx} above 1 k Ω , well into the smoother breakdown regime beyond the sharp rise, we find a crossover to quadratic dependence $\delta\rho_{yx} \propto \rho_{xx}^2$, which has been seen previously in temperature-driven measurements in a QAH system [7]. We have also performed these measurements at higher temperatures, finding a faster rise in $|\delta\rho_{yx}|$ with increasing ρ_{xx} , and checked that longitudinal and Hall measurements do not differ substantially between different pairs of contacts [29].

D. Current distribution in the breakdown regime

An interesting question related to the onset of significant dissipation with breakdown is how the current is distributed in the device. Following Büttiker's model of the QH effect [60], the QAH effect is usually described with an edge state picture (as we have introduced it here), and one proposed source of dissipation at low temperatures is the additional presence of nonchiral edge states [13]. However, although much of the QAH literature holds that the entire current in transport experiments is carried in the edge channels, this is not necessarily the case; 2D bulk states below the Fermi level may also carry a nonzero current density, as has been shown in QH, even in the regime of linear response where the edge state picture can be used to correctly predict conductances [61]. Moreover, at high currents in QH samples under conditions optimized for metrology, current flows predominantly in the bulk [19,49,62], and the BSEH model discounts edge-transport effects in breakdown. Indeed, pure edge transport in the QAH effect appears inconsistent with our results. If current flow in the device resulted purely from a density difference in oppositely propagating edge states, we would expect a strong enhancement of dissipation due to tunneling between the edge states and the surface states as the chemical potential difference between the edges, $\Delta\mu = (h/e)I$, approached the size of the gap [49]. The gap extracted from the fit to thermal activation would predict such an edge conduction breakdown at only ~ 5 nA, strongly hinting that the bulk also plays a role at

the higher currents measured here, even in the prebreakdown, low-dissipation regime.

For further insight on this point, we consider the geometrical scaling of this effect. For breakdown based on edge conduction alone, the breakdown current I_{cr} should be relatively independent of the Hall bar width W in the transverse direction. If instead bulk conduction is dominant and approximately homogeneous, we would expect $I_{cr} \propto W$, and dissipation as measured by V_{xx} should scale with the distance L between voltage contacts. Indeed, in the QH effect, current flow in the bulk leads to linear scaling of I_{cr} with W for samples that are sufficiently large compared to relevant length scales (e.g., scale of density fluctuations) [49]. Thus, measuring the size dependence of breakdown behavior can provide additional clues to the nature of the current distribution.

On a separate chip from the same film growth as device 1, we fabricated three additional devices of varying size and measured longitudinal voltage as a function of current. These Hall bars are 100 μm wide with one square between voltage terminals, 100 μm wide by six squares, and 10 μm wide by ten squares (devices 2A, 2B, and 2C, respectively). Each device was measured with the gate voltage tuned to the approximate center of the resistivity plateau (respectively for devices 2A–2C: -7 V, -5.8 V, -6.65 V), at a value of V_g chosen because it minimized ρ_{xx} measured at an elevated temperature [29]. To account for the geometrical differences between the Hall bars, the average longitudinal electric field $E_x = V_{xx}/L$ is plotted against the average current density $j_x = I_x/W$ in Fig. 3(d). In each case, there is a sharp increase in E_x at around $j_x = 1.2$ nA/ μm indicating the expected linear dependence of breakdown current on width, and the behavior of $E_x(j_x)$ in the breakdown regime appears to be nearly independent of sample size. Based on this geometrical scaling, we infer that breakdown must take place through bulk conduction. We note that the strength of these conclusions is limited by the small number of samples, although Kawamura *et al.* [12] have similarly observed that the characteristic current for crossover from low V_{xx} to a higher-dissipation, linear I - V regime is roughly proportional to sample width.

IV. DISSIPATION IN THE PREBREAKDOWN REGIME

An explanation for behavior in the prebreakdown regime, before the sharp increase in dissipation, is less clear. $E_x(j_x)$, shown in Fig. 3(d), is also similar for the three Hall bars in prebreakdown, suggesting that bulk conduction may be involved. However, it does not appear to be as uniform between the devices as in breakdown itself: E_x values differ by a factor of up to 4 for similar j_x . Intriguingly, in the original (and lowest temperature) cooldown of device 1 we observed a power-law relationship between V_{xx} and I_x over nearly 1 order of magnitude in current and 4 orders of magnitude in voltage [Fig. 3(a)]. A fit between 25 nA and 100 nA yields $V_{xx} \propto I_x^{6.4}$. Power-law scaling of voltage with current is known to occur for tunneling into QH edge states [63], but for $\nu = 1$, the closest analog to the QAH state, both theory and experiment find $V \propto I$. In the absence of bulk conduction, Luttinger liquid behavior due to the possible presence of additional, quasi-helical edge states theoretically predicted in some QAH systems could perhaps lead to a different power-law scaling. However, in

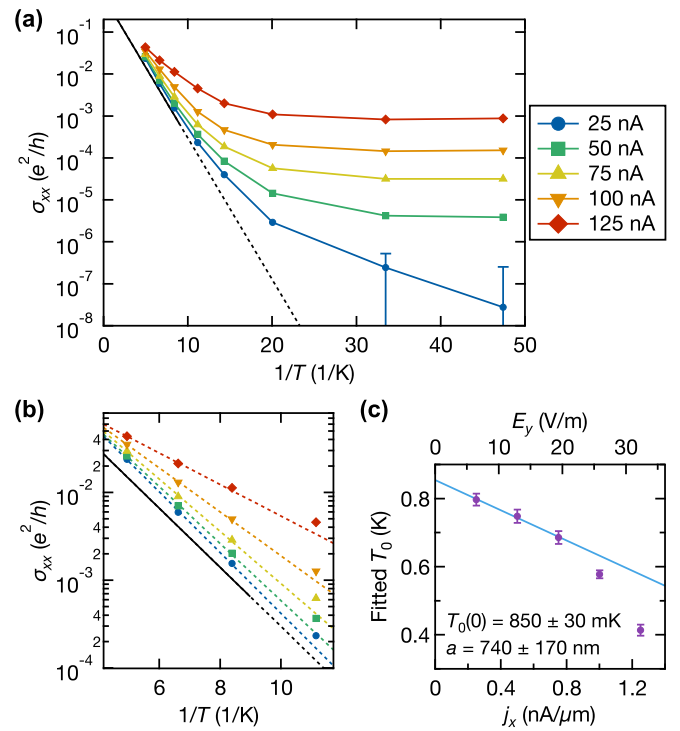


FIG. 4. Temperature dependence of σ_{xx} for $V_g = -7.5$ V. (a) Arrhenius plot of the temperature dependence of σ_{xx} in device 1 for five bias currents between 25 nA and 125 nA. The conductivity appears relatively temperature independent below 50 mK, while above 100 mK it may be thermally activated, although we cannot rule out variable-range hopping conduction based on the temperature dependence alone. The black solid line shows the fit to thermal activation for measurements with a lock-in amplifier at 5 nA ac bias current [Fig. 1(d), inset], and the dashed line extrapolates the fit to lower temperatures. (b) Detailed view of σ_{xx} vs $1/T$ for higher temperatures, with fits to activated conductivity (colored dashed lines) for measurements above 100 mK. (c) Fitted activation temperature scale T_0 as a function of current density j_x or transverse electric field $E_y \approx (h/e^2)j_x$. A fit (blue line) to $T_0(E_y) = T_0(0) - aeE_y/k_B$ for $j_x \leq 0.75$ nA/ μm yields $T_0(0) = 850 \pm 30$ mK and $a = 740 \pm 170$ nm.

contrast to the power law in device 1, measurements of devices 2A–2C at a slightly higher temperature show clear curvature in the log-scale plot of E_x versus j_x [Fig. 3(d)], and the computed σ_{xx} appears exponential in j_x below breakdown [29]. In any case, our evidence for current flow in the bulk suggests this explanation is unlikely, though evaluating the role of nonchiral edge states, if they exist, in prebreakdown, nonohmic conduction may be better addressed in future experiments using nonlocal measurements and alternative device geometries.

A. Low-temperature behavior

Measurements of V_{xx} as a function of current and temperature up to the onset of breakdown in device 1 provide additional hints about the prebreakdown behavior. In Fig. 4(a), we display these data as σ_{xx} in an Arrhenius plot for I_x between 25 nA and 125 nA. For $T \leq 50$ mK, σ_{xx} is nearly temperature independent, particularly for higher currents. At least two explanations are plausible. First, even before a runaway heating effect causes a sharp breakdown, the electron system may be slowly heated

above the lattice temperature in the prebreakdown regime. If σ_{xx} is nonzero, then the electron temperature must rise slowly as the current and therefore the heating rate increase in order for the rate of heat loss to the lattice to rise correspondingly. The apparent temperature independence could result from the electron temperature being sufficiently elevated that varying the lattice temperature has little effect in this range. In the BSEH model, this would correspond to $Z(T_L) \ll Z(T_e)$ in Eq. (1) for T_L under ~ 50 mK and sufficiently large current. Second, the behavior of σ_{xx} at low temperature may be dominated by hopping transport driven by the Hall electric field (recalling that $E_y = \rho_{yx} j_x \approx j_x h/e^2$). In QH systems, nonohmic conduction at the lowest temperatures and high but subcritical currents has been ascribed to field-driven VRH of the form $\sigma_{xx}(I_x) = \sigma_{xx}^I \exp(-\sqrt{E_1/E_y})$, where E_1 is a characteristic field and the prefactor σ_{xx}^I is only weakly dependent on temperature and field [19,40,64]. Field-driven VRH has also been proposed [12] as an explanation of the current dependence of σ_{xx} in the QAH effect, and a fit of our low-temperature data to such a model is plausible [29]. Whether or not temperature-independent hopping is responsible for part of the prebreakdown behavior, however, the presence of the breakdown effect indicates that a crossover must take place to a regime in which electron heating is the dominant effect.

B. Field-assisted thermal activation model

At elevated temperatures, σ_{xx} clearly has a strong temperature dependence. Above 100 mK, higher current dc measurements can be plausibly fit to thermal activation, shown in a detailed view in Fig. 4(b), but transport is still clearly nonohmic. Although for each current alone, the temperature dependence of the conductivity in this range can be reasonably fit to thermally driven VRH with $\sigma_{xx} \propto \exp[-(T_1/T)^{1/(d+1)}]$ for $d = 1, 2, \text{ or } 3$, the typical model for nonohmic VRH does not clearly agree with the data [29]. Instead, the similar form $\sigma_{xx} \propto \exp(-T_0/T)$ that matches both lock-in and dc measurements suggests activated conduction is more likely. In Fig. 4(c), we plot the fitted thermal activation temperature scales from these data against j_x and E_y , showing the reduction in T_0 with increasing E_y .

In prebreakdown QH, a linear reduction in the activation energy with Hall electric field has frequently been observed and suggested to be caused by either a field-dependent broadening of the Landau level extended state bands [65] or the tilted potential over the length scale of localized state wave functions reducing the energy required for excitation to extended states [51]. The latter explanation may also apply in a QAH system for excitations to the surface-state bands from midgap, disorder-localized states at the Fermi level, or perhaps from the edge states. If this is the case, the field E_y applied over the relevant length scale a should reduce the activation energy by aeE_y , so we fit the data for lower currents, $j_x \leq 0.75$ nA/ μm , to $T_0(E_y) = T_0(0) - aeE_y/k_B$. The fit yields $T_0(0) = 850 \pm 30$ mK, somewhat larger than the 780-mK scale found in lock-in measurements, but in reasonable agreement, and $a = 740 \pm 170$ nm, where we assume a uniform distribution of current in the bulk in order to estimate E_y . Although $T_0(E_y)$ departs from this dependence at higher fields, the nonlinearity could be due to electron heating

near the onset of breakdown causing the thermal activation fit to be inaccurate.

The value of a derived from this fitting is fairly consistent with that extracted from a fit of data at fixed temperature: in devices 2A–2C, $\sigma_{xx} \propto \exp(aeE_y/k_B T)$, with $a \approx 600$ nm, in the prebreakdown regime for $j_x \leq 1$ nA/ μm [29]. The physical interpretation of the length scale a is unclear, but if this behavior is caused by excitations from disorder-localized states in the gap, a may be the associated localization length. If it instead results from transitions from the edge states, a likely reflects the characteristic length scale $\lambda = \hbar v_F/\Delta$ for the decay of the edge state wave function into the bulk (although edge effects may invalidate our assumption of spatially uniform E_y). Using the gap extracted from thermal activation at low current, we estimated this length earlier as ~ 4 μm , larger than the fitted value of a but within an order of magnitude.

C. Summary of prebreakdown dissipation

Based on our interpretation, the temperature and current dependence of the conductivity we have observed in the prebreakdown regime appears to result from an interplay of electron heating and dissipation in the bulk. Slow heating of the electron system, before the thermal runaway in breakdown, is likely the dominant factor in determining $\sigma_{xx}(j_x)$ at high currents and low lattice temperatures, and should be enhanced by the electric-field-dependent dissipation processes we have discussed. These mechanisms of field-assisted thermal activation to the surface-state bands and possible field-dependent VRH may govern the behavior of the conductivity at lower currents or higher temperatures where electron heating plays less of a role. As other authors [12,17] have suggested, a better understanding of localization and the origin of midgap states in QAH systems will be important for further investigation of this dissipation in the pursuit of more robust quantization.

V. CONCLUSION

In summary, we have demonstrated that the QAH effect presents a promising platform for resistance metrology with accurate quantization of the Hall resistance to within one part per million at zero magnetic field. The primary limitation to the precise measurement of quantization at low temperatures is a current-induced breakdown of the low-dissipation state, which we attribute to runaway electron heating in bulk current flow. Though currently available materials show strong temperature dependence, and the small gap leads to breakdown at significantly smaller currents than in QH samples, new material systems [26,27] and improved growth techniques [9] to increase the exchange-induced gap, reduce disorder in the gap size, or lower the density of midgap states may make QAH metrology more practical. With existing materials, our results suggest Hall bar arrays or simply wider Hall bars will allow for higher current and therefore lower noise measurements of quantization. Further study may also elucidate the complicated prebreakdown behavior of the conductivity we have observed here.

Note added. After submission we became aware of work by Götz *et al.* reporting measurements of Hall resistance in V-doped $(\text{Bi,Sb})_2\text{Te}_3$ with similar precision and accuracy of quantization [66].

ACKNOWLEDGMENTS

We thank Marlin Kraft for performing resistance standard calibrations at NIST, and Marc Kastner, Biao Lian, Shoucheng Zhang, Dan Shahar, and Assa Auerbach for helpful discussions. Device fabrication, measurements, and analysis were supported by the U.S. Department of Energy, Office of Science, Basic Energy Sciences, Materials Sciences and Engineering Division, under Contract No. DE-AC02-76SF00515. Infrastructure and cryostat support were funded in part by the Gordon and Betty Moore Foundation through Grant No. GBMF3429. X.K., L.P., and K.L.W. acknowledge support from FAME, one of six centers of STARnet, a Semiconductor Research

Corporation program sponsored by MARCO and DARPA, and from the Army Research Office under Grants No. W911NF-16-1-0472 and No. W911NF-15-1-0561:P00001. X.K. acknowledges support from the Chinese National Thousand Young Talents Program and Shanghai Sailing Program under Grant No. 17YF1429200. Part of this work was performed at the Stanford Nano Shared Facilities (SNSF), supported by the National Science Foundation under Award No. ECCS-1542152. Identification of commercial products or services used in this work does not imply endorsement by the U.S. government, nor does it imply that these products are the best available for the applications described.

- [1] R. Yu, W. Zhang, H.-J. Zhang, S.-C. Zhang, X. Dai, and Z. Fang, *Science* **329**, 61 (2010).
- [2] Y. L. Chen, J.-H. Chu, J. G. Analytis, Z. K. Liu, K. Igarashi, H.-H. Kuo, X. L. Qi, S. K. Mo, R. G. Moore, D. H. Lu, M. Hashimoto, T. Sasagawa, S. C. Zhang, I. R. Fisher, Z. Hussain, and Z. X. Shen, *Science* **329**, 659 (2010).
- [3] J. G. Checkelsky, J. Ye, Y. Onose, Y. Iwasa, and Y. Tokura, *Nat. Phys.* **8**, 729 (2012).
- [4] C.-Z. Chang, J. Zhang, X. Feng, J. Shen, Z. Zhang, M. Guo, K. Li, Y. Ou, P. Wei, L.-L. Wang, Z.-Q. Ji, Y. Feng, S. Ji, X. Chen, J. Jia, X. Dai, Z. Fang, S.-C. Zhang, K. He, Y. Wang, L. Lu, X.-C. Ma, and Q.-K. Xue, *Science* **340**, 167 (2013).
- [5] J. G. Checkelsky, R. Yoshimi, A. Tsukazaki, K. S. Takahashi, Y. Kozuka, J. Falson, M. Kawasaki, and Y. Tokura, *Nat. Phys.* **10**, 731 (2014).
- [6] X. Kou, S. T. Guo, Y. Fan, L. Pan, M. Lang, Y. Jiang, Q. Shao, T. Nie, K. Murata, J. Tang, Y. Wang, L. He, T. K. Lee, W. L. Lee, and K. L. Wang, *Phys. Rev. Lett.* **113**, 137201 (2014).
- [7] A. J. Bestwick, E. J. Fox, X. Kou, L. Pan, K. L. Wang, and D. Goldhaber-Gordon, *Phys. Rev. Lett.* **114**, 187201 (2015).
- [8] A. Kandala, A. Richardella, S. Kempinger, C.-X. Liu, and N. Samarth, *Nat. Commun.* **6**, 7434 (2015).
- [9] M. Mogi, R. Yoshimi, A. Tsukazaki, K. Yasuda, Y. Kozuka, K. S. Takahashi, M. Kawasaki, and Y. Tokura, *Appl. Phys. Lett.* **107**, 182401 (2015).
- [10] C.-Z. Chang, W. Zhao, D. Y. Kim, H. Zhang, B. A. Assaf, D. Heiman, S.-C. Zhang, C. Liu, M. H. W. Chan, and J. S. Moodera, *Nat. Mater.* **14**, 473 (2015).
- [11] S. Grauer, S. Schreyeck, M. Winnerlein, K. Brunner, C. Gould, and L. W. Molenkamp, *Phys. Rev. B* **92**, 201304 (2015).
- [12] M. Kawamura, R. Yoshimi, A. Tsukazaki, K. S. Takahashi, M. Kawasaki, and Y. Tokura, *Phys. Rev. Lett.* **119**, 016803 (2017).
- [13] J. Wang, B. Lian, H. Zhang, and S.-C. Zhang, *Phys. Rev. Lett.* **111**, 086803 (2013).
- [14] C.-Z. Chang, W. Zhao, D. Y. Kim, P. Wei, J. K. Jain, C. Liu, M. H. W. Chan, and J. S. Moodera, *Phys. Rev. Lett.* **115**, 057206 (2015).
- [15] M. Liu, W. Wang, A. R. Richardella, A. Kandala, J. Li, A. Yazdani, N. Samarth, and N. P. Ong, *Sci. Adv.* **2**, e1600167 (2016).
- [16] I. Lee, C. K. Kim, J. Lee, S. J. L. Billinge, R. Zhong, J. A. Schneeloch, T. Liu, T. Valla, J. M. Tranquada, G. Gu, and J. C. S. Davis, *Proc. Natl. Acad. Sci. USA* **112**, 1316 (2015).
- [17] W. Li, M. Claassen, C.-Z. Chang, B. Moritz, T. Jia, C. Zhang, S. Rebec, J. J. Lee, M. Hashimoto, D.-H. Lu, R. G. Moore, J. S. Moodera, T. P. Devereaux, and Z.-X. Shen, *Sci. Rep.* **6**, 32732 (2016).
- [18] Z. Yue and M. E. Raikh, *Phys. Rev. B* **94**, 155313 (2016).
- [19] B. Jeckelmann and B. Jeanneret, *Rep. Prog. Phys.* **64**, 1603 (2001).
- [20] W. Poirier and F. Schopfer, *Eur. Phys. J. Spec. Top.* **172**, 207 (2009).
- [21] R. Ribeiro-Palau, F. Lafont, J. Brun-Picard, D. Kazazis, A. Michon, F. Cheynis, O. Couturaud, C. Consejo, B. Jouault, W. Poirier, and F. Schopfer, *Nat. Nanotechnol.* **10**, 965 (2015).
- [22] M. W. Keller and J. Aumentado, *Physics* **9**, 144 (2016).
- [23] H. Scherer and B. Camarota, *Meas. Sci. Technol.* **23**, 124010 (2012).
- [24] J. Brun-Picard, S. Djordjevic, D. Leprat, F. Schopfer, and W. Poirier, *Phys. Rev. X* **6**, 041051 (2016).
- [25] X. Feng, Y. Feng, J. Wang, Y. Ou, Z. Hao, C. Liu, Z. Zhang, L. Zhang, C. Lin, J. Liao, Y. Li, L. L. Wang, S. H. Ji, X. Chen, X. Ma, S. C. Zhang, Y. Wang, K. He, and Q. K. Xue, *Adv. Mater.* **28**, 6386 (2016).
- [26] Y. Xu, B. Yan, H.-J. Zhang, J. Wang, G. Xu, P. Tang, W. Duan, and S.-C. Zhang, *Phys. Rev. Lett.* **111**, 136804 (2013).
- [27] S.-C. Wu, G. Shan, and B. Yan, *Phys. Rev. Lett.* **113**, 256401 (2014).
- [28] F. Fischer and M. Grayson, *J. Appl. Phys.* **98**, 013710 (2005).
- [29] See Supplemental Material at <http://link.aps.org/supplemental/10.1103/PhysRevB.98.075145>, which includes Refs. [30–39], for further information about methods, a discussion regarding measuring Hall resistance larger than the quantized value, additional supporting data, and fits to variable-range hopping models.
- [30] F. P. Milliken, J. R. Rozen, G. A. Keefe, and R. H. Koch, *Rev. Sci. Instrum.* **78**, 024701 (2007).
- [31] F. Delahaye and B. Jeckelmann, *Metrologia* **40**, 217 (2003).
- [32] Y. Yang, L.-I. Huang, Y. Fukuyama, F.-H. Liu, M. A. Real, P. Barbara, C.-T. Liang, D. B. Newell, and R. E. Elmquist, *Small* **11**, 90 (2015).
- [33] A. L. Efros and B. I. Shklovskii, *J. Phys. C* **8**, L49 (1975).
- [34] B. I. Shklovskii, E. I. Levin, H. Fritzsche, and S. D. Baranovskii, in *Transport, Correlation and Structural Defects*, edited by H. Fritzsche (World Scientific, Singapore, 1990).
- [35] M. Pollak and I. Riess, *J. Phys. C* **9**, 2339 (1976).
- [36] S. M. Grannan, A. E. Lange, E. E. Haller, and J. W. Beeman, *Phys. Rev. B* **45**, 4516 (1992).

- [37] C.-I. Liu, B.-Y. Wu, C. Chuang, Y.-C. Lee, Y.-J. Ho, Y. Yang, R. E. Elmquist, S.-T. Lo, and C.-T. Liang, *Semicond. Sci. Technol.* **31**, 105008 (2016).
- [38] G. Ebert, K. von Klitzing, K. Ploog, and G. Weinmann, *J. Phys. C* **16**, 5441 (1983).
- [39] S. Marianer and B. I. Shklovskii, *Phys. Rev. B* **46**, 13100 (1992).
- [40] M. Furlan, *Phys. Rev. B* **57**, 14818 (1998).
- [41] D. Drung, M. Götz, E. Pesel, J.-H. Storm, C. Aßmann, M. Peters, and T. Schurig, *Supercond. Sci. Technol.* **22**, 114004 (2009).
- [42] D. Drung, M. Gotz, E. Pesel, H. J. Barthelmeß, and C. Hinrichs, *IEEE Trans. Instrum. Meas.* **62**, 2820 (2013).
- [43] J. Säiler, A. Wild, V. Lang, A. Siddiki, and D. Bougeard, *New J. Phys.* **12**, 113033 (2010).
- [44] W. V. D. Wel, C. J. P. M. Harmans, and J. E. Mooij, *J. Phys. C* **21**, L171 (1988).
- [45] Y. Yang, G. Cheng, P. Mende, I. G. Calizo, R. M. Feenstra, C. Chuang, C.-W. Liu, C.-I. Liu, G. R. Jones, A. R. Hight Walker, and R. E. Elmquist, *Carbon* **115**, 229 (2017).
- [46] F. Delahaye, *J. Appl. Phys.* **73**, 7914 (1993).
- [47] W. Poirier, A. Bounouh, F. Piquemal, and J. P. André, *Metrologia* **41**, 285 (2004).
- [48] D. Drung and J.-H. Storm, *IEEE Trans. Instrum. Meas.* **60**, 2347 (2011).
- [49] G. Nachtwei, *Physica E* **4**, 79 (1999).
- [50] S. Komiyama and Y. Kawaguchi, *Phys. Rev. B* **61**, 2014 (2000).
- [51] S. Komiyama, T. Takamasu, S. Hiyamizu, and S. Sasa, *Solid State Commun.* **54**, 479 (1985).
- [52] L. Eaves and F. W. Sheard, *Semicond. Sci. Technol.* **1**, 346 (1986).
- [53] D. Jena, T. Fang, Q. Zhang, and H. Xing, *Appl. Phys. Lett.* **93**, 112106 (2008).
- [54] N. Ma and D. Jena, *Appl. Phys. Lett.* **102**, 132102 (2013).
- [55] J. Zhang, C.-Z. Chang, Z. Zhang, J. Wen, X. Feng, K. Li, M. Liu, K. He, L. Wang, X. Chen, Q.-K. Xue, X. Ma, and Y. Wang, *Nat. Commun.* **2**, 574 (2011).
- [56] S.-Y. Xu, M. Neupane, C. Liu, D. Zhang, A. Richardella, L. Andrew Wray, N. Alidoust, M. Leandersson, T. Balasubramanian, J. Sánchez-Barriga, O. Rader, G. Landolt, B. Slomski, J. Hugo Dil, J. Osterwalder, T.-R. Chang, H.-T. Jeng, H. Lin, A. Bansil, N. Samarth, and M. Zahid Hasan, *Nat. Phys.* **8**, 616 (2012).
- [57] L. Q. Duong, T. Das, Y. P. Feng, and H. Lin, *J. Appl. Phys.* **117**, 17C741 (2015).
- [58] M. Ovadia, B. Sacépé, and D. Shahar, *Phys. Rev. Lett.* **102**, 176802 (2009).
- [59] M. E. Cage, R. F. Dziuba, B. F. Field, E. R. Williams, S. M. Girvin, A. C. Gossard, D. C. Tsui, and R. J. Wagner, *Phys. Rev. Lett.* **51**, 1374 (1983).
- [60] M. Büttiker, *Phys. Rev. B* **38**, 9375 (1988).
- [61] C. W. J. Beenakker and H. van Houten, *Solid State Phys.* **44**, 1 (1991).
- [62] J. Weis and K. von Klitzing, *Phil. Trans. R. Soc. A* **369**, 3954 (2011).
- [63] A. M. Chang, L. N. Pfeiffer, and K. W. West, *Phys. Rev. Lett.* **77**, 2538 (1996).
- [64] D. G. Polyakov and B. I. Shklovskii, *Phys. Rev. B* **48**, 11167 (1993).
- [65] T. Shimada, T. Okamoto, and S. Kawaji, *Physica B* **249-251**, 107 (1998).
- [66] M. Götz, K. M. Fijalkowski, E. Pesel, M. Hartl, S. Schreyeck, M. Winnerlein, S. Grauer, H. Scherer, K. Brunner, C. Gould, F. J. Ahlers, and L. W. Molenkamp, *Appl. Phys. Lett.* **112**, 072102 (2018).